PROCEEDINGS, 41st Workshop on Geothermal Reservoir Engineering
Stanford University, Stanford, California, February 22-24, 2016
SGP-TR-209

Monitoring Fluid-Rock Interactions at In-Situ Conditions Using Computed Tomography

Mathias Nehler, Thomas Andolfsson, Ferdinand Stöckhert, Jörg Renner, Rolf Bracke

Lennershofstraße 140, 44801 Bochum

mathias.nehler@hs-bochum.de

Keywords: CT scanning, Core flooding experiments, Hydrothermal alteration, Core holder

ABSTRACT

The experimentally investigation of the physic-chemical interactions of fluids, rocks and the cementation of geothermal wells is the main goal of the project. The influence of hydrothermal alteration on rock properties like permeability, thermal conductivity and thermal diffusivity is under investigation for typical rock samples like the Bentheim sandstone as well as carboniferous silt- and sandstones of the Ruhr area (Ruhr Sandstone) in Germany. This will help to predict the long-term reservoir development and increase the efficiency of geothermal power plants. The measurements will be performed with newly configured, laboratory devices. A computer tomography-scanner (CT scanner) with a multi-focal x-ray tube of 225 kV for resolutions of around 1 µm (best case scenario) is used for CT scanning. It is possible to scan rock cores up to 600 mm in length and from less than 3 mm up to 100 mm in thickness by the helix CT scanning method. The computerized tomography is a non-destructive technique, which provides 3D reconstructed images of absorbing materials by reconstruction algorithms. Simulation software will enable the 3D visualization combined with numerical simulation capabilities to compute physical properties of the analyzed materials such as absolute permeability and porosity or thermal conductivity. The CT scanning unit will be extended with a setup for flow through experiments at high pressures up to 25 MPa and temperatures up to more than 150°C to simulate reservoir conditions. Pressure gauges and mass flow meters allow the calculation of the effective permeability, which can be compared directly to the results calculated by the scanning software. The segmentation of typical alteration processes (e.g. dissolution and precipitation) will be optimized in the first place. This includes the improvement of imaging quality within the CT scanner by developing a prototype core-holder consisting of layered aluminum and/or carbon fiber epoxy for optimal X-ray scans. In addition the research is focused on the preparation of synthetic brines representing the saline fluids of the northern German basin.

1. INTRODUCTION

X-ray computed tomography (CT) is a common non-destructive three-dimensional imaging method. Earth scientists use it in their quest for three-dimensional information on rock microstructures that enhances understanding of physical processes taking place at micro-scale, i.e., on porous media. In this paper we focus on the establishment of a complete laboratory setup to perform computed tomography under in-situ HP/HT conditions to simulate geothermal reservoirs. The idea is to get more information for the construction of medium to deep geothermal heat storage facilities and the long-term stability of the exploited reservoirs.

The main objective is the still ongoing implementation of a standard laboratory method, which is focused on fractured or porous systems and their geochemical and geomechanical behavior due to circulating fluids. Therefor the laboratory setup is explained in detail with the actual workflow. The paper shows on different rock samples how the porosity and permeability can be determined and how results could be obtained and evaluated. Flow through experiments and the CT scanning process will be explained in detail.

2. ROCK SAMPLING AND PREPARATION

For the proposed testing procedures sandstone varieties were sampled. The sandstone varieties used for the experiments are from different locations worldwide representing typical sandstones concerning composition, grain size, degree of sorting and maturity of the sandstones. Therefore, these sandstones differ also in porosity and permeability. But none of the used sandstone blocks showed any traces of significant bedding or macroscopic anisotropy.

Polished thin sections were prepared of all samples for microscopic analysis. Mineral determination was done with the Axio Scope.A1 Zeiss polarization microscope and the keyence VHX-2000 digital microscope by including semiautomatic calculations with the VHX-2000 software by the means of threshold analysis. But due to the complexity of textures and the mineral appearance artifacts occurred.

Furthermore, samples were grinded to powder for XRD analysis. Diffraction patterns were recorded in reflection geometry with an Empyrean Theta-Theta diffractometer (Panalytical, Almelo) equipped with a copper tube, 0.25° divergent slit, 0.5° antiscatter slit (incident beam), 7.5 mm high antiscatter slit (diffracted beam), incident and diffracted beam 0.04 rad soller slits, and a position sensitive PIXcel-1d detector. The K-beta emission line is suppressed by a Ni Filter. For qualitative phase analysis the specimens were scanned in the 5-80° 2θ range with a step width of 0.0131° and 250 s collection time at an ambient temperature of T = 300 K. The ICDD powder diffraction file (PDF2) in conjunction with the HighScore Plus software (Panalytical, Almelo) was used for qualitative phase analysis.

2.1 Geological Decription

The so-called Ruhr- (RS,RSS), the Fontainebleau- (FS) and the Bentheim- (GBS) sandstone (sst) as well as a graywacke (Ambr) were used for first measurements.

The Bentheim (GBS) sandstone is a very homogeneous, well sorted, usually yellow coloured quartz arenite from the Romberg quarry next to Bad Bentheim (Germany). The average grain size is 250 µm. The sandstone was deposited during the lower Cretaceous in a basin north of the London-Brabant Massif and the Rhenish Massif in a shallow marine environment (Kemper, 1976). The GBS sandstone is mainly comprised of quartz (around 90 %), minor K-feldspar or microcline and rare clay minerals. Rarely opaque minerals occur representing iron-rich minerals such as hematite or pyrite.

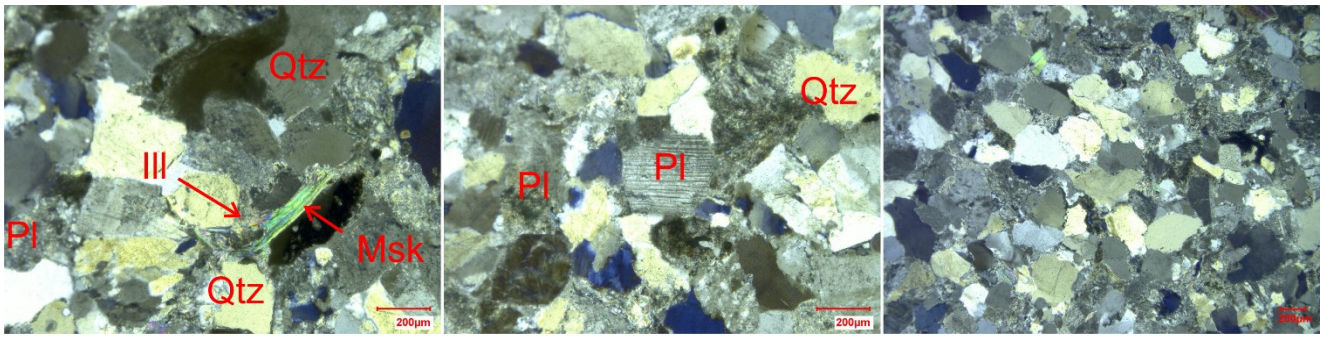

Figure 1: The cross-polarized photos shows the typical Ruhr sandstone with sub-angular quartz grains. Typical is partial replacement of the muscovite by illite (left) and sericitic alteration of plagioclase, which can be recognized by brownish colors and cloudy appearance. In addition polysynthetic twinning can be seen (middle).

The grey Ruhr (RS) sandstone is a carboniferous sandstone from the Namur B to Westfal A (Upper Carboniferous), which was deposited in the Variscan foredeep in a fluvio-deltaic environment and buried and folded during Variscan orogeny (Karg, 2005; Jasper, 2010). The arkosic sandstone is a fine to medium grained grey sandstone with interlayering of silt- and mudstones. The thickness of the layers ranges from decimetre to meter scale. The sub-angular to angular grains have an average grain size of 200 µm. The RS sandstone consists of abundant quartz of around 60 % and plagioclase (approx. 35 %) with minor chlorite. Chlorite as well as illite can account for up to 5 %. The plagioclase is heavily altered to sericite (sericitization), which can be distinguished by cloudy appearance.

The Fontainebleau (FS) sandstone is a regional widespread shallow buried unit of around 50 to 60 m thickness of the Ile de France region, France of Oligocene (Stampian) age (Haddad, 2006 , French, 2013). The FS sandstone is a fine grained, grain supported, very well sorted quartz arenite. The subangular grains have grain diameters of about 150 µm. Rarely kaolinite occur and secondary amorphous or micro-crystalline quartz can be distinguished (French, 2013).

The graywacke is mined in the quarry of Ambrock south of Hagen, Germany. In this area these middle Devonian (Eifel) rocks of the Brandenberg sequence are genuine (Jorand, 2015). Samples are characterized by a typical dark greyish, greenish colour and a very fine grained matrix consisting of quartz, feldspar and sericite.

3. LABORATORY SETUP

In the following the experimental setup is explained in detail. First the CT Scanning procedure is stated and afterwards the proposed experiments, which were only partly fulfilled and are still in process.

3.1 CT Scanner

CT scanning or X-ray computerized tomography is a non-destructive method, which provides reconstructed 3-D images (Kak, 2001). The technique was developed in the 1970s for medical purposes (Alkadhi, 2011). The method is based on the absorption of X-rays when they pass through a solid object e.g. a rock sample. The attenuation of the X-rays follows the Lambert-Beer´s Law, where I denote the attenuated intensity after the X-rays have passed through an object. X is the length of the object, I_0 is the initial intensity and μ is the linear attenuation coefficient. The linear attenuation coefficient depends explicitly on the number of atoms encountered by the X-ray beam. The visibility of the different features depends always on the spatial resolution of the images and on the contrast of the features compared to the surrounding features.

$$I = I_0 \cdot e^{x\mu} \tag{1}$$

Reconstruction algorithms translate the attenuation coefficients into grey value images. The X-ray intensity is measured by the counts on the detector for a given object position and termed a view (Ketchman, 2003). Multiple sets of views are obtained from an object over a range of angular orientations to generate two-dimensional images that are called slices. Therefore each scanned slice of the sample will be divided in a matrix of so called voxels (3-D volume elements). The attenuation coefficient is determined for each voxel and depict as a mediate grey value in a 2-D picture. To get 3-D data the object is rotated (or the detector and X-ray source rotate) within the beam and a large number of two-dimensional scans is created at different angles. The three-dimensional distribution of attenuation coefficients is back-calculated to reconstruct the scanned volume (Wildenschild, 2013). The patterns are characteristic for the materials of the sample like minerals and fluids.

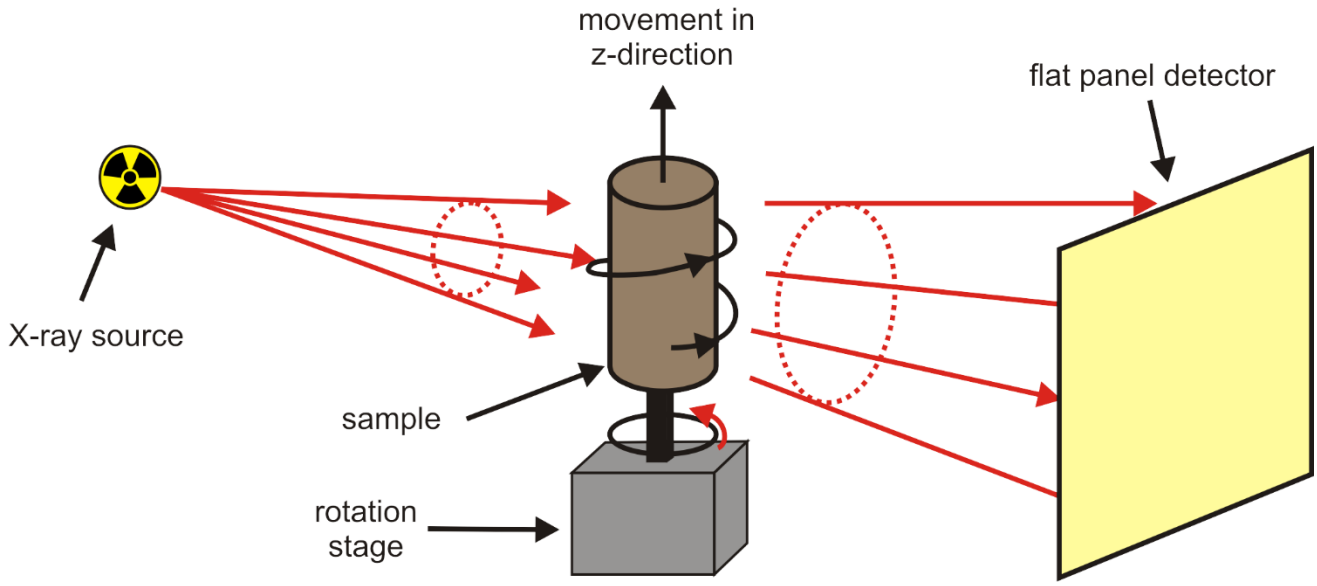

Figure 2: Tomography set-up for helix cone beam microCT system (modified after (Wildenschild, 2013)

In the experimental set-up a custom designed CT scanner based on the CTalpha, which was manufactured by PROCON X-RAY, was used. The general functional principle of the cone-beam tomography system is illustrated in Figure 2. As usual the sample is positioned on a rotational stage in between the X-ray source and the flat panel detector. In addition the system is equipped with a helical option (also improperly called "spiral scanning") to create helical CT scans due to translation of the object in z-direction, while rotating. This allows to measure samples up to 600 mm in length. In addition the method reduces artefacts known as Feldkamp artefacts (Kruth, 2011) and increases the resolution along the axis of rotation.

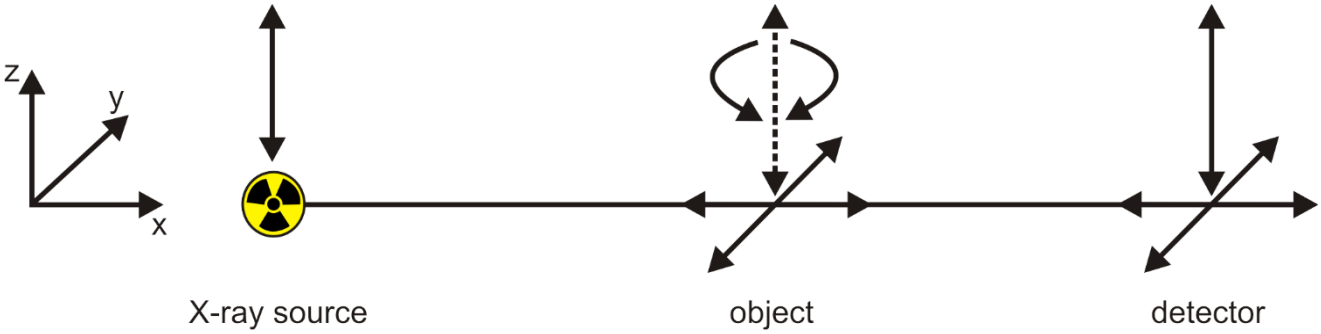

Figure 3: Mechanical configuration of the CT system with movement axes.

A solid microgabbro foundations hosts the different system components such as X-ray source, rotation table and detector as well as structures for flow through experiments. The mechanical axes (see Figure 3) allow the movement of the object and detector in the direction of the x-axis giving a high amount of flexibility for optimizing CT scanning parameters such as spatial resolution (magnification). The object movement in y-direction enables the alignment of the system, while the positioning of the detector along the the y-axis allows for an extension of the field of view. The vertical translation of the X-ray source and the detector along the z-axis leads to a virtual movement of the object along the z-axis.

The open X-ray source is the high energy microfocus X-ray transmission tube XWT-225-THE PLUS produced by X-RAY WorX. The target power is 50 Watt. The tube can be used with voltages between 30 up to 225 kV (only standard 230 V is necessary) and is designed for nano-, micro- and high-power mode in dependency of the needs. The minimal focal spot is around 0.25 µm (JIMA resolution) for powers below 2 Watt (nano-mode). The Varian 14 bit flat-panel detector is 190 x 240 mm in size with 1515 x 1900 pixels for X-ray detection. For the reconstruction of the generated CT scans a cluster is implemented with 96GB RAM.

3.2 Scanning Configuration

The samples are placed at an optimal position between the x-ray source and the detector to enhance resolution (see also Figure 3). The number of angles, which is required for high quality images was at least 1200 but usually 1600.

Beam-hardening is an effect which is caused by the greater attenuation of low energy photons compared to high energy photons. This results in a brighter corona structure at the edges of samples than the center (Jovanovic, 2013, Ketchman, 2003, Kruth, 2011). To reduce these effect it is possible to use thin filter plates consisting of copper, brass or aluminium in varying thickness. The filter cuts out the low energy photons, so that only the hard spectrum of the X-rays is used to perform the measurements. This enables a better surface

edge detection, but reduces simultaneously the intensity and can therefore worsen the signal to noise ratio. Compensation of this effect can be done by increasing the exposure time (Kruth, 2011). Typically a 1 mm aluminium plate was used if a beam hardening filtering was necessary.

3.3 Reconstruction

The reconstruction of the obtained raw-datasets (sinograms) was done with Volex software developed by the Fraunhofer Institute, Germany and is based on filtered back projections and the Feldkamp algorithm. During the reconstruction process the raw intensity data is converted to CT numbers or CT values. The range of these so called grey values (CT numbers) is determined by the computer system. In our case not more the grey values are between 0 and 56000. To maximize the CT grey value contrast it is important to select the optimal reconstruction parameters. This means to stretch the lowest and highest values over the available 14-bit range and to ensure not to lose important data by overshooting the limits (see also Ketchman, 2003). In addition the ring-artefact reduction algorithm of the Volex software was used to detect vertical lines within the sinograms of the raw data and remove them prior reconstruction. These ring-artefacts are commonly caused by shifts of the rotation centre in relation to the detector and are indicated as full or partial circles in the reconstructed slices (Anas. 2011, Bernard, 2006, Sadi, 2010, Stock, 1999). Otherwise no further unnecessary algorithms were implemented to keep the reconstructed data as rawly as possible.

3.4 Post Processing

After reconstruction the datasets were loaded into the commercial software AvizoFire, Version 9.0.1 by FEI for further processing and filtering. If needed or wanted sub-volumes of the samples were selected with following advantages:

- Reduction of computational time.
- Excluding parts of the reconstructed data which are affected by scanning artefacts such as beam hardening.
- To avoid mechanically damaged parts at the outside of the samples.

Main purpose of the post-processing is to reduce the image noise by performing one or more consecutive filter operations on the grey-scale images to simplify the following segmentation. A bunch of methods for edge-preserving noise reductions are implemented in Avizo Fire or have been published (Buades.2005, Kaestner, 2008). For this work the selection was restricted to two very common and widely used filters. The Median Filter and the Non-local means Filter. Both filters can be used either in 2-D or 3-D mode. Later results in longer computational times but shows better results.

Median Filter

Edge detection is usually based on the analysis of intensity differences within pixel neighborhoods (Lopez-Molina, 2014). The filter replaces voxels by using the approximated median of neighboring voxels in a user defined area in 2-D or 3-D. This removes noise at the cost of unavoidable smoothing the edges (Gallagher, 1981, Welk, 2007). The filter works fine when images contain non-Gaussian noise and very small artefacts. The smoothing module uses a low-pass filter to reduce the contrast and soften the edges of objects. The grey values become brighter. Existing peaks of the data histogram will be sharpened and become more distinct afterwards (Lopez-Molina, 2014, Wildenschild, 2013). It is also robust against outliers.

Non-local means Filter

The Non-local means Filter uses a function of the weighed Euclidean distance to determine the similarity between all other pixels in a given search window (Buades, 2005a). The new value for each voxel is determined by the weighed distribution of the pixels within the search window. The final weights are calculated by applying a Gauss kernel. The non-local means Filter is more robust compared to the Median Filter meaning that smaller, thinner features at the boundaries of different materials will be preserved, while the other parts will be simplified by smoothing (Buades, 2005a, Buades, 2005b). The filter works best on white noise.

3.5 Segmentation

The edge (surface) detection or segmentation is a mandatory step to capture the geometry of the important features for further analysis. Frequently this means binarization of the images into just two materials (e.g. pore space and solid grains), which are represented by black (zero) and white (one). On the other hand it can be more complex by separating into n-different phases e.g. air, water, oil, minerals etc. If it is relevant for the research question. The choice of the best method depends on the number and size of phases to separate and how easy the phase segmentation can be fulfilled (Kaestner, 2008).

Very often the segmentation is based on grey-value thresholding. This means the boundary between two phases is defined by a discrete value. The problem is that the edge voxel gray value can change within a sample due to beam hardening effects or the so called “partial volume effects” (Kruth, 2011). Also the values for boundaries of systems with three and more phases will differ depending on the transition from material to material. Hence simple thresholding by using the “iso-50 value” between two maxima of the grey-value histogram usually fail. The edge is often shifted with respect to the real material edge and user defined (manual) grey-value thresholding is necessary to improve segmentation quality.

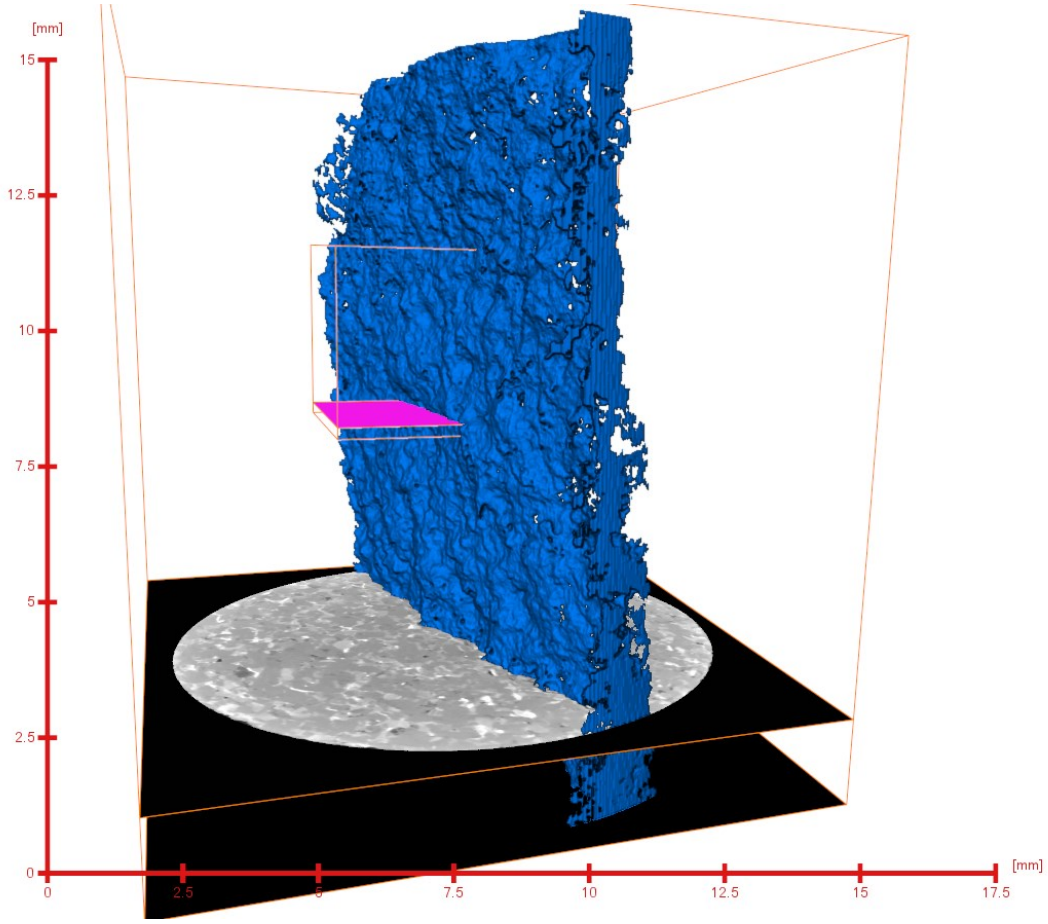

Figure 4: Segmentation of a fracture (extension crack) of Ruhr sandstone sample. Only the smaller box (purple) of 400x400x400 voxels is used for further quantification to reduce computational time.

3.5 Core Flooding Unit for Flow Through Experiments

The CT scanning unit is extended with a setup for flow through experiments at high pressures up to 250 bar (momentarily) and temperatures up to more than 150°C to simulate reservoir conditions. Pressure gauges and mass flow meters allow the calculation of the effective permeability, which can be compared directly to the results calculated by the scanning software (Ott et al., (2012)). A pair of ISCO 260D pumps is used for providing the confining medium, which can be oil or water as well as heat. Another pair of ISCO 500D pumps is used for liquid feeding. These piston pumps are made of hastelloy C276 and can be used with corrosive as well as volatile fluids. The pumps can be used in different modes depending on the experimental needs.

- Continuous Flow Mode: Liquid from a reservoir is pumped continuously by both pumps. One pump is always refilling while the other is pumping.
- Single Constant Pressure Mode: One single pump keeps the pressure constant.
- Single Constant Flow Mode: One single pump is pumping a constant volume per time or receiving a constant volume per time.
- Combination of Single Constant Pressure Mode and Single Constant Flow Mode with two pumps.

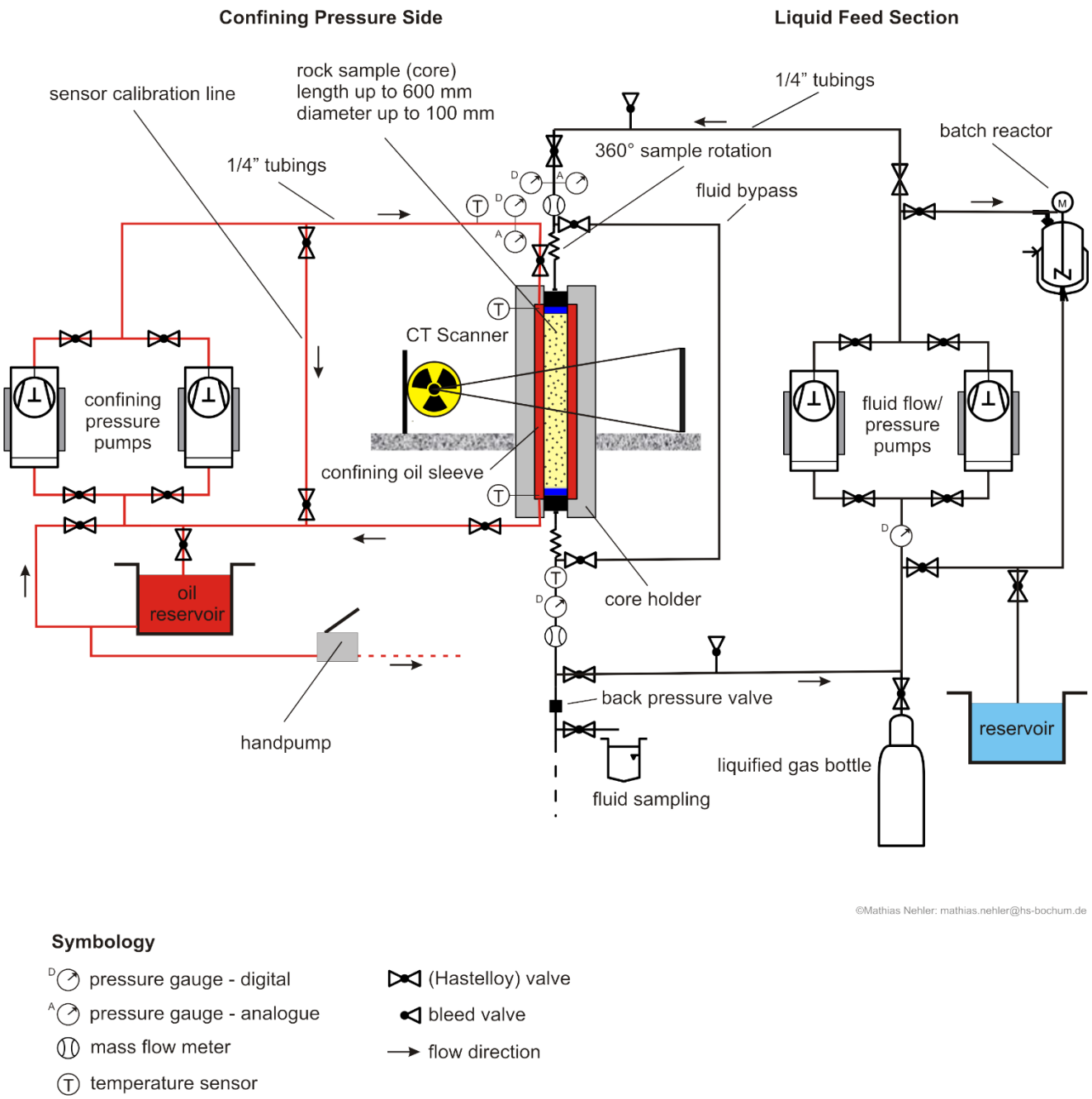

Figure 5: Experimental setup of the planned fluid-circulation unit, which is combined with a CT scanner.

In Figure 5 an overview of the general laboratory setup is shown including the pumping system for flow through experiment and the CT scanner as the central unit. Usually the experiments are performed with the ISCO 260D pumps providing the pressure for confinement, while both ISCO 500D pump are used in pressure mode with different pressures in dependency of the sample permeability. Due to a pressure gradient a flow through the samples will be established after certain amount of time (steady state) and the permeability can be calculated after Darcy.

Core Holder

The core holder is a crucial part of the system to perform experiments under in-situ HP/HT conditions. The core holder was designed with utmost flexibility and security in mind. The requirements are to withstand the working pressures, temperatures and fluids. A modular based assembly allows an easy exchange of parts and the adaptation of the core holder in numerous different experimental set-up. In our case the core holder is used for long-term flow through experiments within and outside of the CT scanner, but it would be also possible to use the cell for example in synchrotron beam-lines.

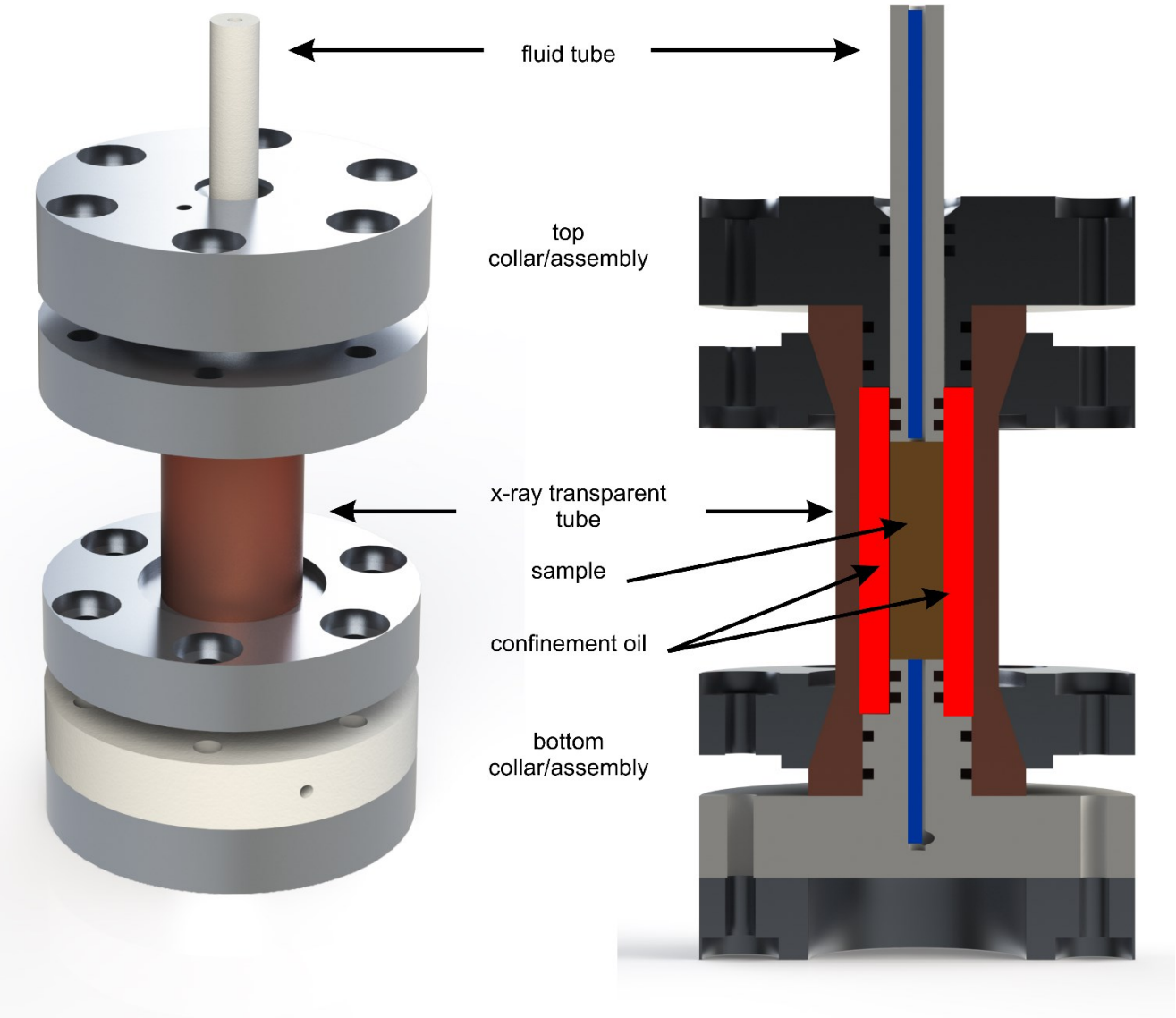

Figure 6: CAD Design of the core holder for 10 mm samples.

The sample size is 10 mm in diameter and 20 up 30 mm in sample length. The sample is mounted centrally inside the X-ray transparent pressure vessel consisting of aluminium (compare to Figure 6). Wetted parts are made of polyether ether ketone (PEEK) a thermoplastic polymer to avoid corrosion due to the usage of highly saline fluids. The sample is fixated between two PEEK tube stubs. The upper tube can be adjusted by a screw on top of the core holder in order to compensate the sample length. 1/8" high pressure standardized chromatography liquid feeding fittings can be connected to the connection ports. While the fittings are limited to a pressure of 35 MPa, the core holder itself is designed for pressures up to 50 MPa. The 1/8" tubing is also made of PEEK. Hence the complete flow-path could be inert, biocompatible and metal-free if needed. At the experimental set-up the flexible PEEK tubes are usually connected to the stationary ¼" tubing's in stainless steel (confining pressure) or hastelloy C276 (liquid feed section).

The core holder is still in an ongoing revision and optimizing process, which includes testing of different materials and exchange of modules. Besides a core holder for samples of 40 mm in diameter and length of up to 500 mm will be manufactured.

3.6 Porosity Measurements

In Addition the total porosity of the samples was derived from a comparison of bulk density and average mineral density. These kind of porosity measurements are pretty much a standard and are used to validate the CT scan results. The bulk density ρ of each prepared sample was calculated from weighing after drying and geometrical volume determination including determinations of the corresponding accuracies, respectively. The matrix densities ρ_m were gained from pycnometer measurements on powders prepared by crushing and grinding the rocks. Standard deviations of the densities as well uncertainties (Gaussian error propagation) were determined (The total porosity ϕ_{tot} derives from the ratio between geometric ρ_g and matrix density ρ_m.

$$\phi_{tot} = 1 - \frac{\rho_g}{\rho_m} \tag{2}$$

3. DATA ANALYSIS

All pressures (liquid feed in/out, confining), temperatures, volume discharge and time are continuously logged with the measuring devices. The data files are than imported to Matlab for further calculations and evaluation of the measurements (see Figure 7). The raw data as well as well some down sampling operations are implemented in the code (e.g. moving average, mean average). For the calculation of the permeability only the mean value of the steady state condition during the experiment is used. The permeability is calculated after Darcy. K denotes the permeability in m^2, η is the viscosity of the fluid, l the length of the sample, A the area vertical to the flow direction and Δp is the pressure difference between inlet and outlet.

$$k = \frac{\eta \cdot l \cdot Q}{A \cdot \Delta p} \tag{3}$$

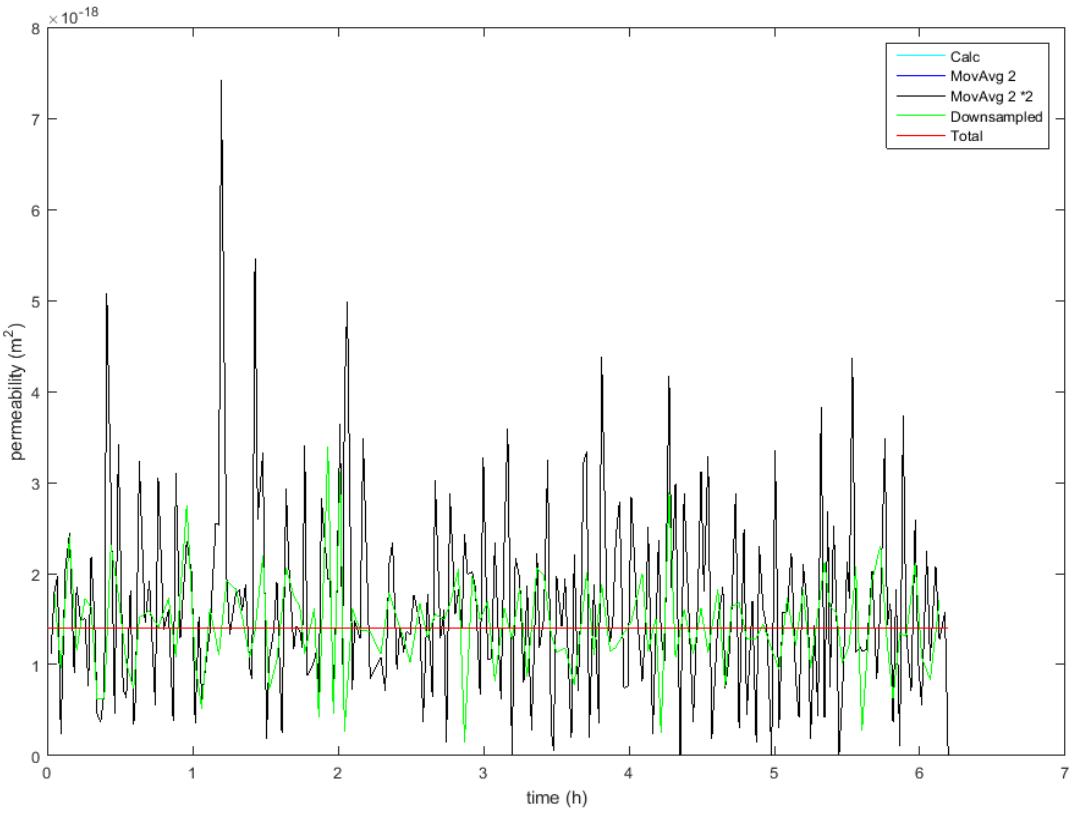

Figure 7: Permeability calculation of a Ruhr sandstone (25 mm length, 10 mm cross-sectional dimension).

The CT data is handled differently. Porosity measurements or volume fraction measurements are done within the software of Avizo, while for further characterization of fractures the segmented data is also imported to Matlab. Every slice of the segmented data is imported to Matlab. In Matlab the fracture is characterized by a set of x,y,z values. The distance to every contact point of fracture and rock matrix is calculated (Figure 8) and hence the surface of the fracture (Figure 9) can be generated. This surface is very complex and therefor simplified with a linear regression in 3-D. Afterwards the mean aperture is calculated and used for an estimation of the permeability.

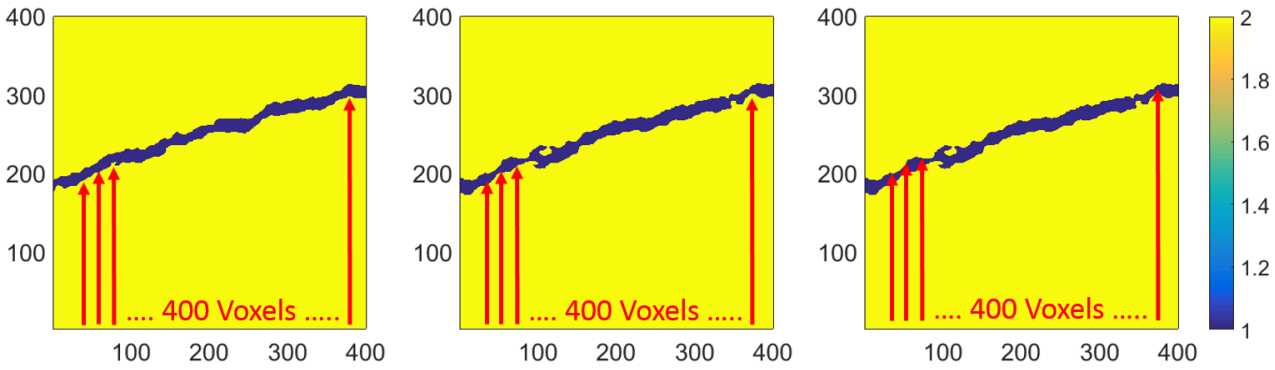

Figure 8: Imported example slices and distance calculation for a cube of 400x400x400 voxels.

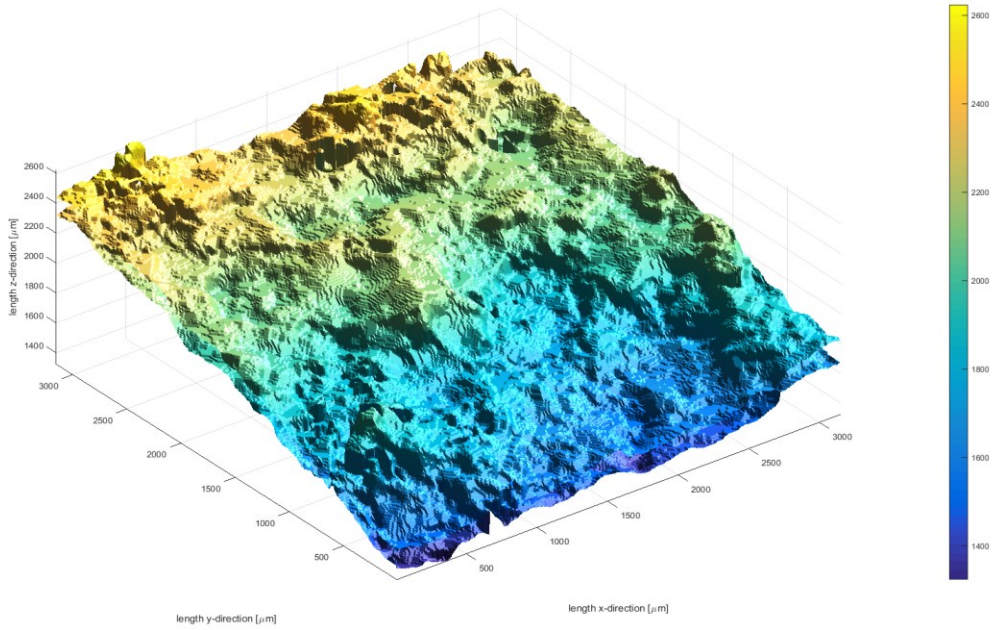

Figure 9: 3D surface data of matrix/fracture boundary for further quantifications.

3. RESULTS

The first permeability measurement results are shown in the table 1 below. The values are in good accordance to literature.

Sample	Size [mm]	Upstream [bar]	Downstream [bar]	deltaP [bar]	Confining [bar]	Flow Q [ml/h]	Permeability [m^2]
Ruhrsandstein	10x20	60.00	5.00	55.00	105	0.03	3.51E-19
Fontainebleau FS9	9.90x20.01	26.03	5.00	21.03	100	30.00	1.01E-15
Fontainebleau FS11	9.78x24.64	39.99	5.02	34.97	75	21.87	4.42E-16
St2	9.46x18.70	4.51	1.00	3.51	50	300.17	6.78E-14
Ruhrsandstein Rst1	9.73x21.24	75.07	1.00	74.07	100	0.13	1.42E-18
Fontainebleau F1	9,74x20,78	75.08	1.00	74.08	100	0.03	3.04E-19
KST2	9.57x21.35	75.08	1.00	74.08	100	0.01	8.18E-20
Fontainebleau FS9-12	10x20	10.00	1.00	9.00	50	96.59	8.51E-15

Table 1: Permeability measurements.

The first measurement of an open fracture was done at an extension crack of a Ruhr sandstone sample (compare to Figure 4). The calculated mean aperture of the linear interpolated fracture surfaces (Figure 10) is 125 µm resulting in an estimated volume flow rate of -7.90E-05 m^3/s of the fracture. This was calculated by using the cubic law for fracture flow.

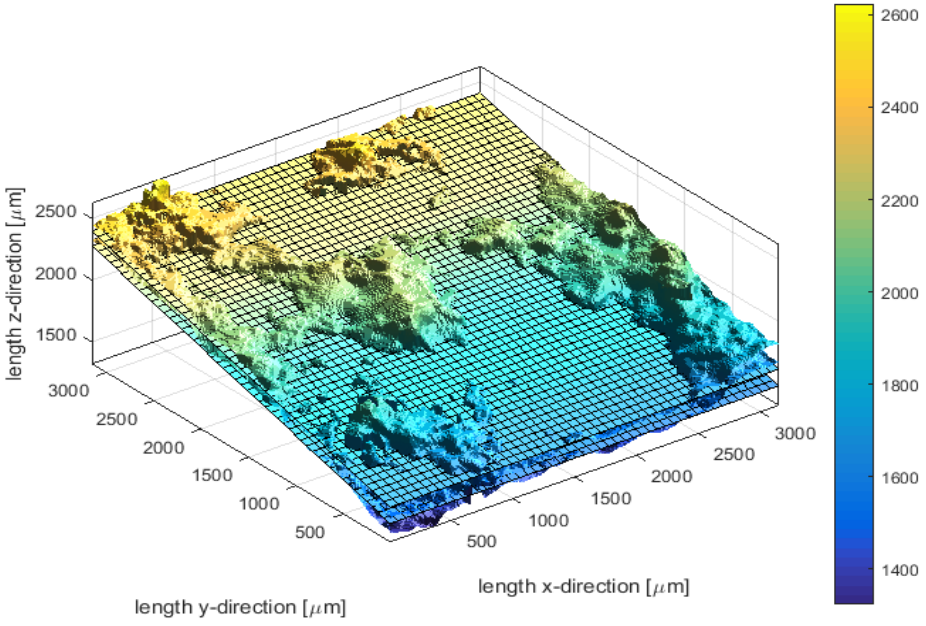

Figure 10: 3D linear regression surface of fracture surfaces.

4. CONCLUSIONS

In general it was shown that the proposed setup works, but until now no measurements were performed inside the CT scanner under higher pressures (more than 2 MPa). The Core Holder is tested und working up to pressures of 25 MPa with PEEK tubings. The CT scanner shows good results. The evaluation of the data is implemented. So everything is in place but further measurements needs to be done to get a statistical data sets.

REFERENCES

Alkadhi, Hatem (2011): Wie funktioniert CT? Eine Einführung in Physik, Funktionsweise und klinische Anwendungen der Computertomographie. Berlin, Heidelberg: Springer.

Anas, Emran Mohammad Abu; Lee, Soo Yeol; Hasan, Kamrul (2011): Classification of ring artifacts for their effective removal using type adaptive correction schemes. In: *Computers in biology and medicine* 41 (6), S. 390–401. DOI: 10.1016/j.compbiomed.2011.03.018.

Bernard, D.; Chirazi, A. (2006): Numerically Enhanced Microtomographic Imaging Method Using a Novel Ring Artefact Filter. In: Jacques Desrues, Gioacchino Viggiani und Pierre Bsuelle (Hg.): Advances in X-ray Tomography for Geomaterials. London, UK: ISTE, S. 117–124.

Buades, A.; Coll, B.; Morel, J. M. (2005): A Review of Image Denoising Algorithms, with a New One. In: *Multiscale Model. Simul.* 4 (2), S. 490–530. DOI: 10.1137/040616024.

Buades, A.; Coll, B.; Morel, J.-M. (2005): A Non-Local Algorithm for Image Denoising. In: 2005 IEEE Computer Society Conference on Computer Vision and Pattern Recognition (CVPR'05). IEEE Computer Society Conference on Computer Vision and Pattern Recognition. San Diego, CA, USA, 20-26 June 2005, S. 60–65.

French, Marsha W.; Worden, Richard H. (2013): Orientation of microcrystalline quartz in the Fontainebleau Formation, Paris Basin and why it preserves porosity. In: *Sedimentary Geology* 284-285, S. 149–158. DOI: 10.1016/j.sedgeo.2012.12.004.

Gallagher, N.; Wise, G. (1981): A theoretical analysis of the properties of median filters. In: *IEEE Trans. Acoust., Speech, Signal Process.* 29 (6), S. 1136–1141. DOI: 10.1109/TASSP.1981.1163708.

Haddad, S. C.; Worden, R. H.; Prior, D. J.; Smalley, P. C. (2006): Quartz Cement in the Fontainebleau Sandstone, Paris Basin, France. Crystallography and Implications for Mechanisms of Cement Growth. In: *Journal of Sedimentary Research* 76 (2), S. 244–256. DOI: 10.2110/jsr.2006.024.

Jasper, K.; Hartkopf-Fröder, C.; Flajs, G.; Littke, R. (2010): Palaeoecological evolution of Duckmantian wetlands in the Ruhr Basin (western Germany). A palynological and coal petrographical analysis. In: *Review of Palaeobotany and Palynology* 162 (2), S. 123–145. DOI: 10.1016/j.revpalbo.2010.06.009.

Jorand, Rachel; Clauser, Christoph; Marquart, Gabriele; Pechnig, Renate (2015): Statistically reliable petrophysical properties of potential reservoir rocks for geothermal energy use and their relation to lithostratigraphy and rock composition. The NE Rhenish Massif and the Lower Rhine Embayment (Germany). In: *Geothermics* 53, S. 413–428. DOI: 10.1016/j.geothermics.2014.08.008.

Jovanović, Zoran; Khan, Faisal; Enzmann, Frieder; Kersten, Michael (2013): Simultaneous segmentation and beam-hardening correction in computed microtomography of rock cores. In: *Computers & Geosciences* 56, S. 142–150. DOI: 10.1016/j.cageo.2013.03.015.

Kaestner, A.; Lehmann, E.; Stampanoni, M. (2008): Imaging and image processing in porous media research. In: *Advances in Water Resources* 31 (9), S. 1174–1187. DOI: 10.1016/j.advwatres.2008.01.022.

Kak, Avinash C.; Slaney, Malcolm (2001): Principles of computerized tomographic imaging. Philadelphia: Society for Industrial and Applied Mathematics (Classics in applied mathematics, 33).

Karg, Harald; Carter, Andrew; Brix, Manfred R.; Littke, Ralf (2005): Late- and post-Variscan cooling and exhumation history of the northern Rhenish massif and the southern Ruhr Basin. New constraints from fission-track analysis. In: *Int J Earth Sci (Geol Rundsch)* 94 (2), S. 180–192. DOI: 10.1007/s00531-005-0467-2.

Kemper, Edwin (1976): Geologischer Führer durch die Grafschaft Bentheim und die angrenzenden Gebiete mit einem Abriss der emsländischen Unterkreide. 5th ed., revised. Nordhorn: Heimatverein der Grafschaft Bentheim (Bentheimer Land, 64).

Ketchman, Richard A.; Carlson, William D. (2003): Acquisition, optimization and interpretation of X-ray computed tomographic imagery: applications to the geosciences. In: F. Mees und Geological Society of London (Hg.): Applications of X-ray Computed Tomography in the Geosciences: Geological Society (Bd. 1), S. 7–22.

Kruth, J. P.; Bartscher, M.; Carmignato, S.; Schmitt, R.; Chiffre, L. de; Weckenmann, A. (2011): Computed tomography for dimensional metrology. In: *CIRP Annals - Manufacturing Technology* 60 (2), S. 821–842. DOI: 10.1016/j.cirp.2011.05.006.

Lopez-Molina, C.; Galar, M.; Bustince, H.; Baets, B. de (2014): On the impact of anisotropic diffusion on edge detection. In: *Pattern Recognition* 47 (1), S. 270–281. DOI: 10.1016/j.patcog.2013.07.009.

Ott, H.; Kloe, K. de; van Bakel, M.; Vos, F.; van Pelt, A.; Legerstee, P. et al. (2012): Core-flood experiment for transport of reactive fluids in rocks. In: *The Review of scientific instruments* 83 (8), S. 084501. DOI: 10.1063/1.4746997.

Sadi, Fazle; Lee, Soo Yeol; Hasan, Md Kamrul (2010): Removal of ring artifacts in computed tomographic imaging using iterative center weighted median filter. In: *Computers in biology and medicine* 40 (1), S. 109–118. DOI: 10.1016/j.compbiomed.2009.11.007.

Welk, Martin; Weickert, Joachim; Becker, Florian; Schnörr, Christoph; Feddern, Christian; Burgeth, Bernhard (2007): Median and related local filters for tensor-valued images. In: *Signal Processing* 87 (2), S. 291–308. DOI: 10.1016/j.sigpro.2005.12.013.

Wildenschild, Dorthe; Sheppard, Adrian P. (2013): X-ray imaging and analysis techniques for quantifying pore-scale structure and processes in subsurface porous medium systems. In: *Advances in Water Resources* 51, S. 217–246. DOI: 10.1016/j.advwatres.2012.07.018.